



# Heterogeneous microstructures tuned in a high throughput architecture

M. Short<sup>a</sup>, J. Müller<sup>a</sup>, S. Lee<sup>a</sup>, H. Fornasier<sup>b</sup>, U. Köhler<sup>b</sup>, V. Ott<sup>a</sup>, M. Stüber<sup>a</sup>, B. Gerdes<sup>c</sup>, T. Rupp<sup>c</sup>, C. Kirchlechner<sup>a</sup>, K. Woll<sup>a</sup>

<sup>a</sup>Institute for Applied Materials, Karlsruhe Institute of Technology (KIT), 76344 Eggenstein-Leopoldshafen, Germany

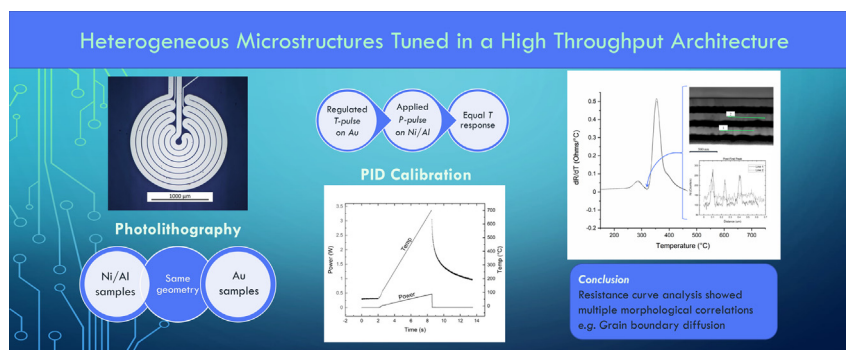
<sup>b</sup>Institute of Microstructure Technology, Karlsruhe Institute of Technology (KIT), 76344 Eggenstein-Leopoldshafen, Germany

<sup>c</sup>Department of Microsystems Engineering (IMTEK), University of Freiburg, 79110 Freiburg, Germany

## HIGHLIGHTS

- Design from Zhang et al. (2018) proposes a resistive heating coil.
- Minimizes heat capacity of sample making temperature solely dependent on input power.
- New method uses PID regulation for improved temporal resolution.
- Method unlocks higher heating rates (~10,000 K/s).
- Method detects microscale morphological changes in Ni/Al thin film.
- Structurally sensitive results complement nanocalorimetry.

## GRAPHICAL ABSTRACT



## ARTICLE INFO

### Article history:

Received 9 November 2022

Revised 6 March 2023

Accepted 14 March 2023

Available online 24 March 2023

### Keywords:

Resistance-temperature sensor  
High-throughput characterization  
Fast thermal pulses  
Microstructure formation  
Nanocalorimetry

## ABSTRACT

A new method applied to the sensor proposed by Zhang et al. in 2018 is demonstrated in this paper that combines the benefits of this design with the fast heating possible with nanocalorimetry. By applying a PID regulated pulse instead of a constant wattage, we unlock an accessible method to sense morphological changes occurring over short time periods that would be invisible to methods based only on heat capacity. In this study, multilayer Ni/Al thin films were linearly heated at 25, 50, 100, and 200 K/s to over 700°C, showing two distinct peaks in resistance change with activation energies of  $55 \pm 4$  and  $74 \pm 7$  kJ/mol, respectively. Through Scanning Transmission Electron Microscopy (STEM) and Energy Dispersive X-ray Analysis (EDX) analysis on cross sections taken ex situ from samples quenched before and after the peaks of interest, we find strong evidence that peak 1 corresponds to Ni diffusing through Al grain boundaries forming intermetallic phases that essentially block the highly conductive Al pathway. This presents the potential to design and calibrate novel heterogeneous structures in a high throughput manner.

© 2023 The Authors. Published by Elsevier Ltd. This is an open access article under the CC BY license (<http://creativecommons.org/licenses/by/4.0/>).

## 1. Introduction

The aim of this paper is to present a method that combines the advantages of nanocalorimetry with the heating chip design proposed by Zhang et al. [1] (shown in Fig. 1) allowing us to unlock more detailed information on morphological changes at fast heating rates than calorimetric methods. Currently the state of the art

method to measure the thermal properties of small samples at fast heating rates is nanocalorimetry [2]. The morphological and phase changes occurring during these rapid temperature pulses have been of scientific interest for some time, some examples of which are studying self propagating reactions [3–6], or silicides for use in the microelectronics industry [7], and have stimulated work into improvements in methodology [8,9] including combinations with

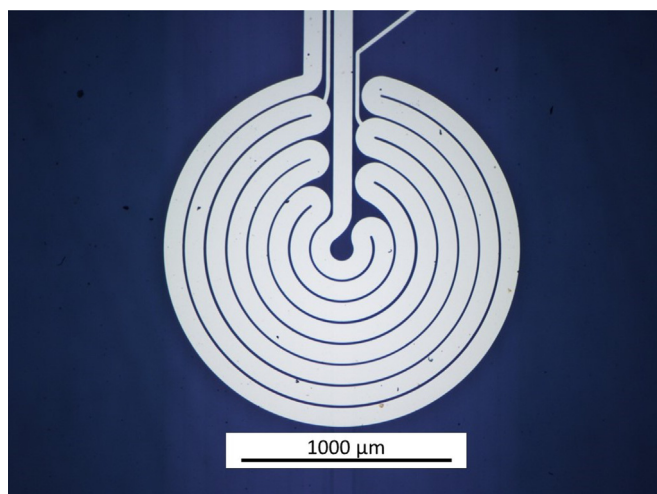


**Fig. 1.** An image of the heating spiral of the calibration sample taken with an optical microscope. The evaporated 15 nm Chrome adhesion layer and 200 nm Gold layer were structured using photolithography on a borosilicate glass substrate. Current was injected through the large leads above the spiral to heat the sample, while the small leads measured the voltage drop across the third ring from the outside to measure the resistance and thereby the temperature.

in situ electron microscopy [10], time resolved X-ray Diffraction (XRD) [11], and mass spectrometry [12] in order to better characterize phase transitions. The general setup, consisting of a platinum heating strip on which the sample is deposited, allows heating rates beyond the million K/s range. As the resistance vs temperature relationship is known, a predetermined voltage pulse can be applied and any deviation from the expected temperature response of the platinum strip can be interpreted as either endo- or exothermic reactions of the deposited sample [13].

The work of Zhang et al. [1] presented a design for an array of sensors that measure the electrical resistance of a sample of interest with respect to its temperature. One key advantage of this design is the low thermal mass of the sample material in comparison with the substrate, making the temperature response solely dependent on the input power irrespective of sample material. After measuring the temperature response of a given constant input power using a sample such as gold with a stable, known temperature vs. resistance relationship, any other conductive sample with the same footprint on the substrate will provide the same response to a small degree of error. As we will demonstrate in this work, measuring the change in resistance instead of heat capacity allowed more sensitive measurements of interesting morphological changes rather than only larger scale phase changes. However, in order to access the fast heating rates provided by nanocalorimetry, what is referred to here as the transient temperature regime, some development had to be done on the heating technique.

The difficulty in investigating the transient temperature regime lies in the unknown nature of heat loss,  $\dot{Q}_{loss}$ . While most of the heating was limited to the chip itself, the increase in temperature of the surrounding chip holding structure was significant enough to necessitate the elimination of any solder lest it evaporate and contaminate the sample. To overcome this, a desired temperature pulse was first calibrated on calibration samples. These consisted of gold deposited in the same geometry as the desired sample, which was then heated to 750°C to stabilize its microstructure and resulting resistance vs. temperature behavior. An image of the heating spiral is shown in Fig. 1.

The resistance vs. temperature behavior was then measured using a hot plate and four point measurement as demonstrated by Zhang et al. These data were then used by a PID regulator to

regulate the current applied to the calibration sample to achieve the desired temperature pulse. This then resulted in a power pulse that could be matched to this temperature pulse. Using the same assumption as Zhang et al. that the thermal mass of the sample was insignificant compared to the substrate, it could be assumed that this power pulse would result in the same temperature pulse for any desired conducting material given the same geometry and substrate.

## 2. Experimental

Borosilicate glass wafers were first cleaned with acetone and isopropanol then treated with hexamethyldisilazane (HMDS) for 30 min. The photoresist Ma-N 1440 (Micro Resist Technology GmbH, Germany) was spin coated at 3000 rpm for 30 s then baked on a hotplate at 100°C for 180 s. The wafers were then exposed to 550 mJ/cm<sup>2</sup> at 365 nm with filter, using a glass photomask with the desired pattern (JD Photo Data, UK). They were then submerged in the developer MaD 533/s (Micro Resist Technology GmbH, Germany) for 120 s and washed with deionized water.

For the gold calibration samples, a 10 nm Cr adhesion layer followed by 200 nm of Au was deposited by electron beam physical vapor deposition using a Univex 450. Gold purity was 99.99%, deposited at a rate of 7–9 Å at a pressure of  $1 \times 10^{-4}$  Pa. The Ni/Al multilayers with 200 nm Al were deposited using magnetron sputtering in a Leybold Z 550 coater (Leybold GmbH, Germany) with a 0.4 Pa Ar atmosphere. Al, Ni, and Ti were deposited at 0.40, 0.69, and 0.31 nm/s for a targeted total of 15 nm Ti (again to promote adhesion to the glass substrate) followed by 3 bilayers of 200 nm Al and 133 nm Ni. STEM analysis shown in Section 3.1.1 revealed an actual layer thicknesses of around 140 nm Ni and 180 nm Al giving a stoichiometric ratio of 54/46 Ni/Al.

For the Ni/Al multilayers with 100 and 300 nm Al layers, a Star 100 Pentaco chamber (FHR Anlagenbau GmbH, Germany) was utilized to deposit the Ti, Ni, and Al using magnetron sputtering. Ar was introduced at 35 sccm resulting in a pressure of 0.5 Pa. Ti and Ni were sputtered at 200 and 300 W resulting in a deposition rate of 3.5 and 6.2 nm/min applied for 4 min 17s and 21 min 27s for a targeted total thickness of 15 and 133 nm, respectively. Al was sputtered at 500 W giving a deposition rate of 11.4 nm/min applied for 8 min 46 s and 26 min 19 s for a targeted total thickness of 100 and 300 nm, respectively. Al and Ni were again arranged in 3 bilayers above the Ti adhesion layer as before. Liftoff was achieved through overnight submergence in a bath of acetone mixing at 1 Hz. The wafers were then diced into the final sample chips and individually checked with an optical microscope for defects such as short circuit bridges.

### 2.1. Temperature vs resistance calibration

The gold calibration chips were stepped across a temperature range from room temperature to 500°C using a copper heating block with a type K thermocouple held onto the surface with a screw. To reduce the thermal gradient from the surface of the copper block and the surface of the chip a metal lid was placed over the top with a small hole to access the electrical contact pads. A low current of 20 mA that was predetermined to have an insignificant heating effect was passed through the heating coil on the chip. The resulting voltage was then used to correlate a temperature versus resistance relationship for the calibration sample.

### 2.2. PID regulator

Fig. 2 shows an example temperature pulse calibrated on a gold sample that increased the temperature linearly at 100 K/s from

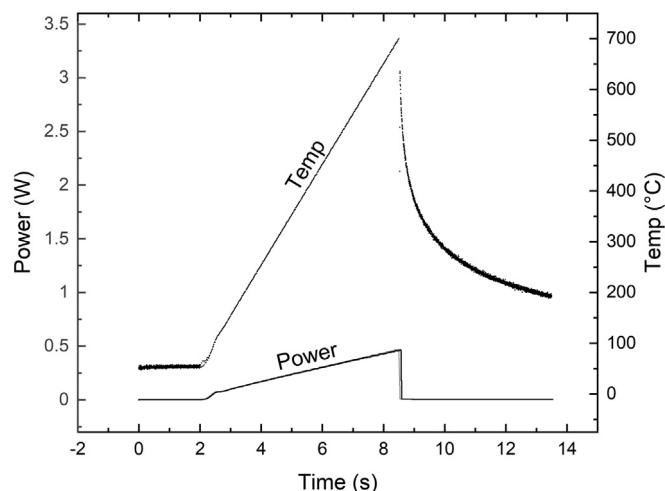


**Fig. 2.** Example temperature curve resulting from the accompanying power pulse applied to gold with a linear temperature ramp of about 100 K/s to 700 °C. The power pulse was PID regulated to match the desired temperature profile. This same power pulse was then applied to a NiAl sample and plotted over the measured power showing very good agreement.

room temperature to 700 °C. Beneath this curve is the power pulse applied to the sample as measured over the ring the small voltage leads are attached to in Fig. 1. In taking the power from this internal ring using a four point measurement rather than over the complete circuit we eliminate sources of error such as different contact resistances between the contact pads on the chip and pins on the sample holder.

By integrating this power pulse we see that the total energy introduced to the ring was approximately 1.4 J. We know the measured ring has a total mass of gold of about 1.3  $\mu\text{g}$ . To heat this to 700°C from room temperature should take approximately  $1.1 \times 10^{-4}$  J, meaning heat loss to the substrate was 4 orders of magnitude greater. This validates our assumption that the specific heat of the sample is an insignificant factor in the temperature vs power relationship.

### 3. Results

The power pulse shown in Fig. 2 when applied to Ni/Al samples resulted in the resistance curves shown in Fig. 3. This data was then smoothed and interpolated with the expected temperature response of the coil also shown in Fig. 2 giving us a relationship of resistance over temperature shown in Fig. 4 on the top. The data shows very good agreement up to around 500°C, after which they diverge likely due to delamination and crack formation resulting in overall destruction of the thin film.

To identify the temperatures where the most significant changes in resistivity occurred, the derivative of this curve was taken which is shown on the bottom. The first small peak at around 60°C was likely an artifact of the initial bump in the calibrated power pulse as the PID regulator stabilized around the desired linear temperature ramp. It was present even in pre-pulsed Ni/Al samples and pre-annealed gold samples where no further structural changes should have taken place. The following two peaks located here at around 285°C and 350°C, consisted of a small initial peak separated by a small gap from a much larger second peak and appeared across our measurements. These will be referred to as peak 1 and 2, respectively. The behavior at higher temperatures became largely inconsistent, oftentimes terminated with a large spike when the coil was destroyed through delamination and/or

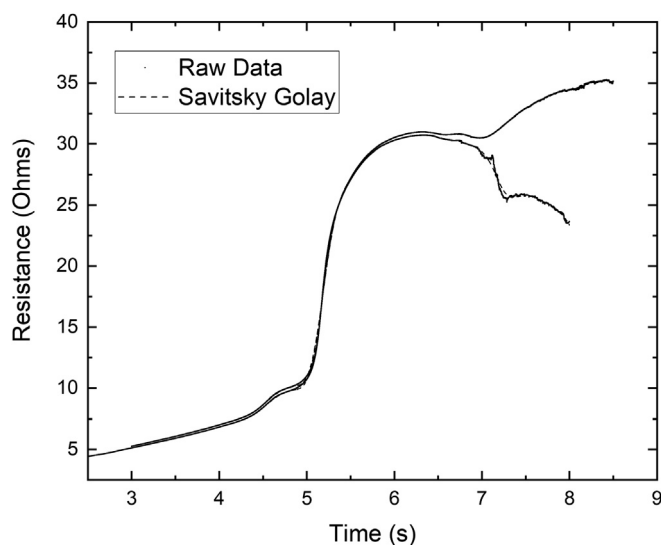


**Fig. 3.** Results of pulsing two identically manufactured Ni/Al samples with the power pulse shown in Fig. 2. The raw data was then smoothed with a Savitsky-Golay filter to make post-processing easier.

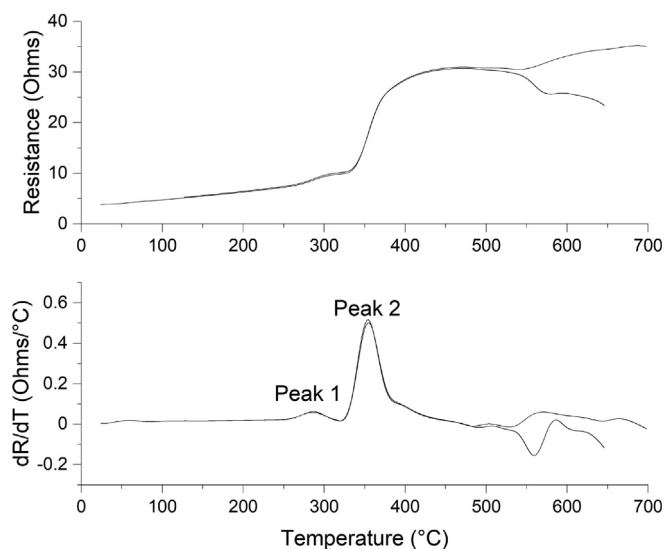


**Fig. 4.** On top is the smoothed resistance data of the Ni/Al samples shown in Fig. 3 interpolated with the expected temperature response shown in Fig. 2 to give a resistance vs. temperature relationship. Below is the gradient of this curve with the two peaks of interest indicated.

crack formation. The evidence for the morphological changes associated with peak 1 and 2 will be elaborated on in the following sections.

#### 3.1. Quenching

Due to the high rate of heat lost to the substrate (only 0.008% of the energy introduced to the sample actually contributed to heating the sample itself), it was possible to rapidly quench the sample at a desired point along the temperature pulse by cutting the power. Fig. 2 demonstrates this rapid reduction in temperature after the current was again reduced to a low 20 mA which allowed continued temperature measurements. This gave us snapshots of the sample as it went through morphological and phase changes which could be used for ex situ Transmission Electron Microscopy (TEM) analysis.

### 3.1.1. STEM

Multiple Ni/Al samples were then heated with the 100 K/s power pulse and then quenched before peak 1, after peak 1, and after peak 2. Cross-sectional TEM lamellae were then taken from each sample, along with an untreated sample, using a Zeiss Cross-beam 550 FIB. STEM images of these lamellae, taken using the built in STEM detector in the same Zeiss Focused Ion Beam (FIB) at 30 kV, are shown in Figs. 5. While the untreated sample shows a clear separation of the Ni and Al layers with little intermixing, already before the first peak we see some phase formation at the interface.

After peak 1 is passed, it seems the morphology doesn't noticeably change. The heterogeneous laminated structure with intermetallic phases at the interface is still maintained. This structure is then lost after peak 2, corresponding to the largest increase in resistance. However, the exact cause of peak 1 remained inconclusive as very large changes in resistivity along the interface would be required to account for the significant change in resistance as it is parallel to the highly conductive Al pathways.

### 3.1.2. EDX Linescans

To investigate the degree of Ni interdiffusion into the Al layer, EDX linescans were taken along the Al film. The results of this taken from the samples quenched before peak 1 and between peak 1 and 2 are shown in Figs. 6 and 7, respectively. Scans were focused on Ni K-alpha activity with the expectation that diffusion of Ni through Al grain boundaries would result in periodic spikes in Ni counts along the scan. Care was taken in the sample quenched before the first peak to scan the middle of the Al layer as well as closer to the Ni interface in order to reveal possible diffusion that

didn't make it all the way through the Al layer. Different background count rates between the two samples can be attributed to different sample thicknesses.

While a small peak is seen in linescan 3 in Fig. 6, it is clear that the linescans shown in Fig. 7 show broader and more frequent Ni peaks. Linescan 3 was also taken fairly close to the Ni interface. We see its sole peak disappear when a scan is taken towards the other side of the Al layer, as shown in linescan 6. Note also that the linescans in Fig. 6 were about twice as long. These results provide good evidence that the major morphological change in the sample over peak 1 is the formation of intermediate phases of Ni and Al within fast diffusion pathways in the Al layers.

### 3.2. Resistivity analysis

In order to find the activation energies of the two different growth mechanisms indicated by peak 1 and 2, samples with Al thicknesses of 100, 200 and 300 nm were each pulsed at 25, 50, 100, and 200 K/s. These data were then organized into Kissinger plots [14] and are shown in Fig. 8. Two measurements were taken at each point to ensure reproducibility. While the peaks shifted to the right as Al film thickness increases, the slopes remained largely consistent, indicating similar activation energies. Indeed, the activation energies for peak 1 were  $51 \pm 6$ ,  $55 \pm 4$ , and  $60 \pm 6$  kJ/mol, while for peak 2 they were  $70 \pm 18$ ,  $74 \pm 7$ , and  $90 \pm 18$  kJ/mol for 100, 200, and 300 nm Al, respectively. While significant variation is present in the values for peak 2, the range given by their respective standard deviations shows agreement with the activation energy Fritz et al. [6] measured for solid state mixing of NiAl multilayer thin films. It should be noted that these activation energies

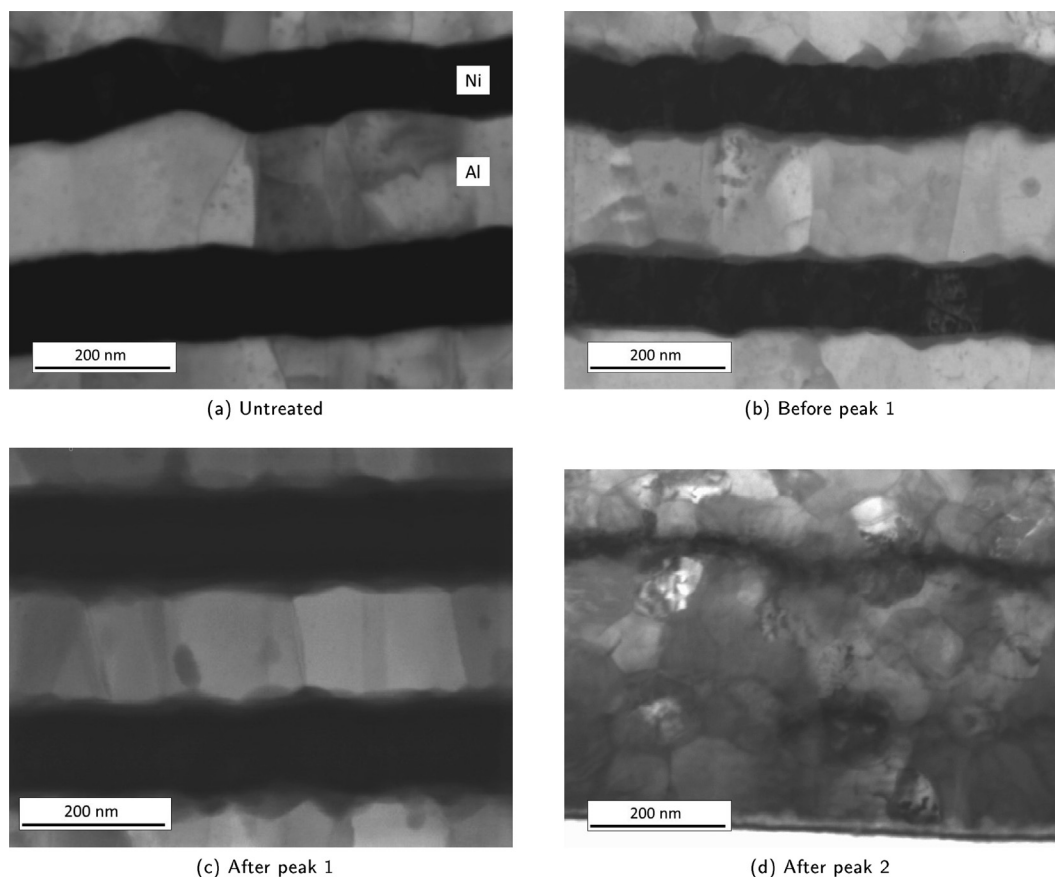


**Fig. 5.** STEM images, all taken at the same magnification, showing the microstructure evolution of the sample after heating at 100 K/s to points indicated relative to the peaks shown in Fig. 4. The darker layers were Ni while the lighter ones were Al as indicated in subfigure a.

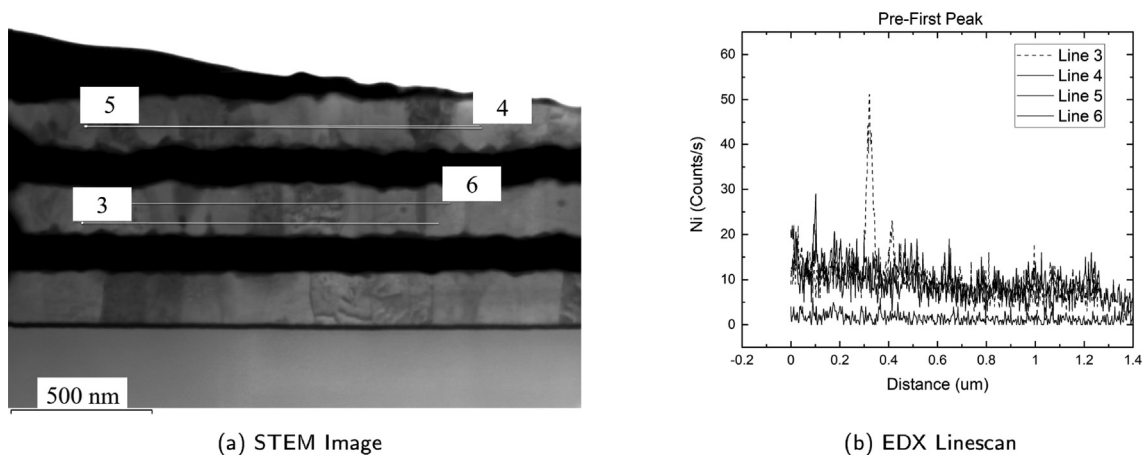


**Fig. 6.** EDX Linescans of Ni activity of sample quenched after 4.146 s placing it immediately before peak 1. On the left is a STEM image of the cross sectional lamella cut from the sample indicating where linescans 3–6 were taken.

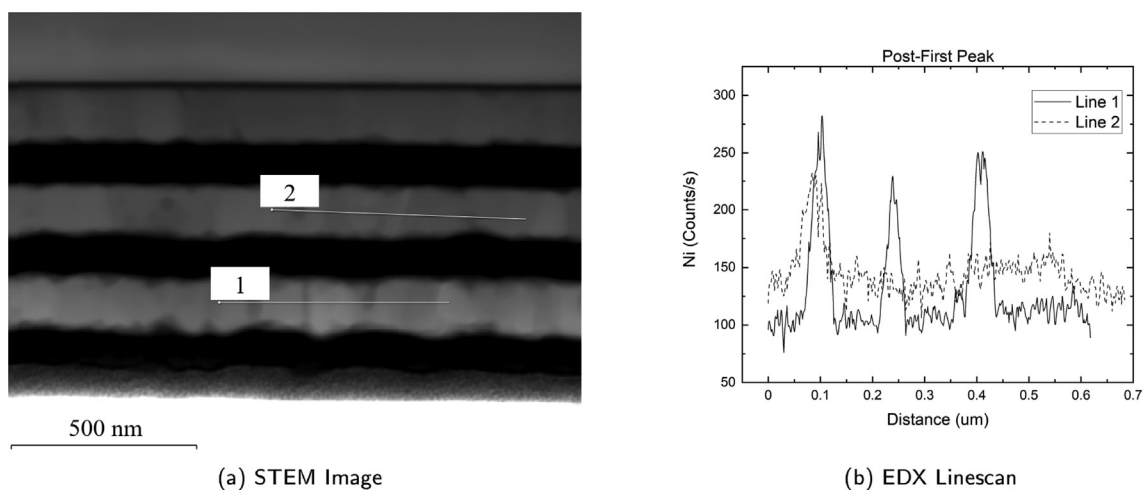


**Fig. 7.** EDX Linescans of Ni activity of sample quenched after 4.766 s placing it immediately after peak 1 and before peak 2. On the left is a STEM image of the cross sectional lamella cut from the sample indicating where linescans 1 and 2 were taken.

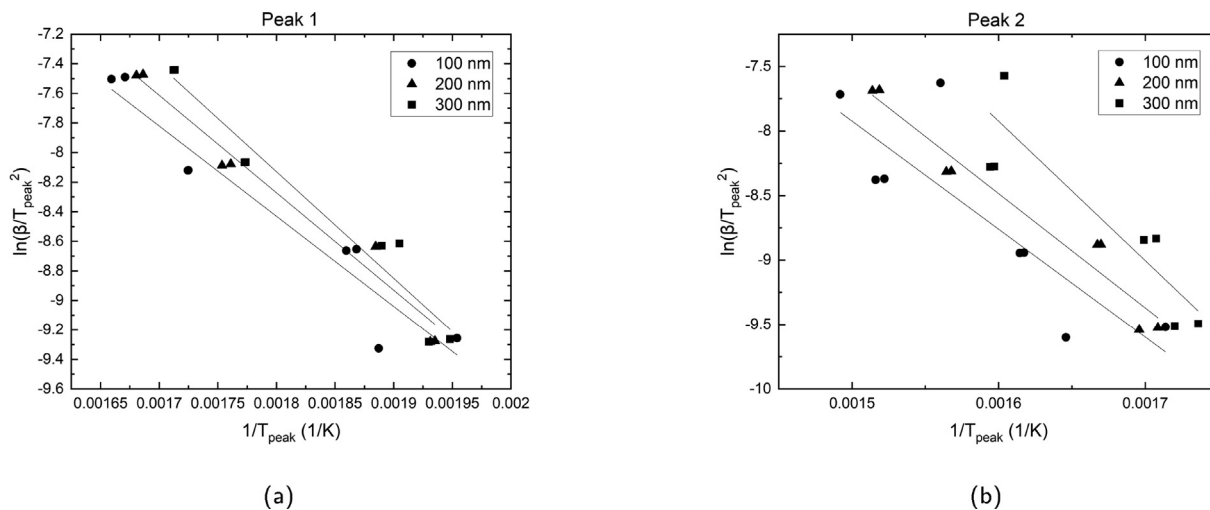


**Fig. 8.** Kissinger plots analyzing the positions of peaks 1 (a) and 2 (b) for samples with 100, 200, and 300 nm Al films. The Ni film remained at 133 nm for all samples.  $\beta$  is the heating rate in K/s.

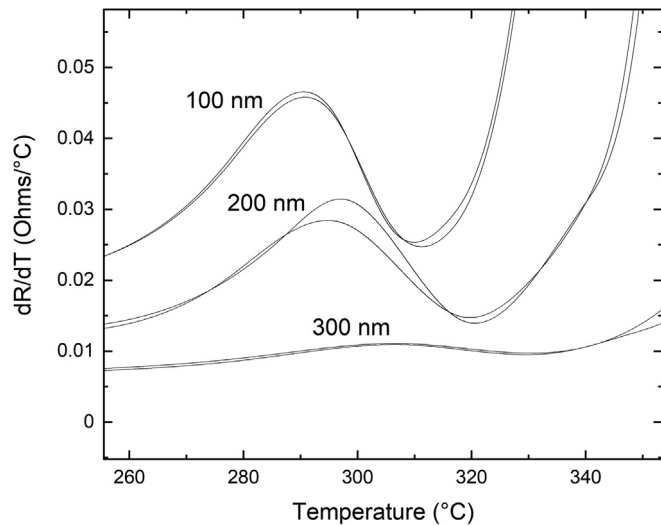


**Fig. 9.** Results for Ni/Al samples pulsed at 100 K/s with three different thin film bilayers of 100, 200, and 300 nm Al films (indicated on the plot) and 133 nm Ni films. The graph is focused on peak 1.

correspond to nucleation *and* diffusion controlled growth [15,16]. Some difference in their values may be accounted for by different stoichiometric ratios as, unlike peak 1, it involves predominantly bulk diffusion and a breakdown of the heterogeneous layered structure.

The data for peak 1 shows a much tighter spread and agreement in activation energies, with a value likely between 50 and 60 kJ/mol. It is interesting to note, however, what happens to the peak shape as the Al thickness is increased, as shown in Fig. 9. While it is expected that the peak position moves up in temperature as it would take longer for Ni to diffuse through the Al grain boundaries, above 200 nm Al it strongly attenuates. This is likely due to the Al film thickness exceeding the average Al grain size, eliminating quick and direct diffusion pathways through the Al layer and creating a more complex network that attenuates its associated quick spike in resistance. This was taken as strong evidence that grain boundary diffusion effects were the culprit for peak 1, rather than a strong change in resistivity of the intermetallic phases along the interface shown in Figs. 5b and 5c.

#### 4. Discussion

Based on the data presented in this manuscript, we describe here our hypothesis on the morphological changes experienced by the Ni/Al sample as they were heated at a constant rate. Fig. 10 shows an example resistance curve (the solid line) from a Ni/Al sample with 3 bilayers of 200 nm Al and 133 nm Ni, heated at 100 K/s. The dotted line below indicated the expected resistance given the geometry of the measured area and the resistivity of Ni and Al with respect to temperature, assuming no phase transformation or diffusion takes place. This was then offset to the dashed line to match the starting resistance measured from the sample to account for resistance contributions from for example interface roughness or grain size.

We see that already before the first peak there is a deviation starting at around 60°C from the resistance expected given only thermal contributions as Ni began to diffuse into the Al layer forming preliminary Ni poor and Ni rich phases on either side of the interface. While the sputtering temperature was not directly measured, it was estimated to be between 50 and 80°C, so the lack of any measureable change below this point is likely because the Ni/Al thin films have already experienced this temperature. The

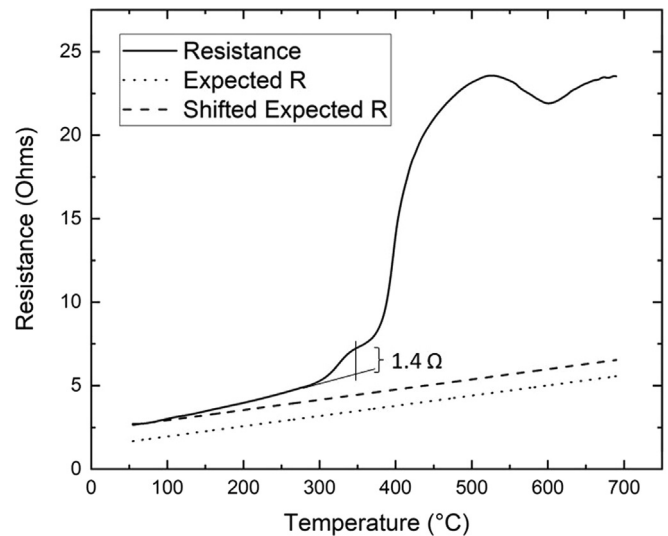


**Fig. 10.** Comparison between a NiAl sample pulsed at 100 K/s with its expected resistance with respect to temperature assuming no phase formation or change in morphology. In order to indicate the degree of resistance change over peak 1, a line is propagated from the data before peak 1 assuming continued linear behavior and compared with the actual resistance measured, giving a difference of about 1.4  $\Omega$ .

continued growth of an intermetallic layer between the Ni and Al layers after this point essentially “throttles” the highly conductive Al layer, gradually increasing overall resistance. Once the activation energy for Ni diffusion through the Al grain boundaries is surpassed, we see a relatively fast spike in resistance (peak 1) as highly resistive intermetallic phases noticeably block current from flowing through the Al. This process runs to a saturation point for a short period before bulk diffusion of Ni into the Al grains begins to dominate and the heterogeneous multilayered structure is lost, eliminating any remaining highly conductive pathways and significantly increasing resistance. After this, there is likely some grain growth as the NiAl phase recrystallizes and stabilizes, which slightly modulates the final resistance until the coil delaminates and cracks.

To evaluate if this hypothesis is realistic, a simplified model was developed as shown in Fig. 11 that could be more easily mathematically simulated. The image represents a cross section of the Ni/Al multilayer along the longitudinal plane, looking from the side of the coil lane. This could then be represented as a circuit diagram,

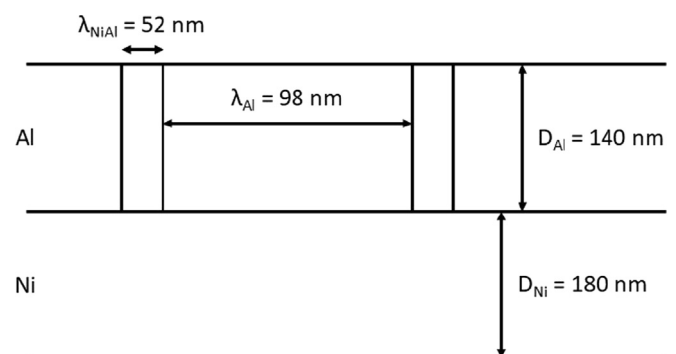


**Fig. 11.** Diagram showing a schematic of one Ni/Al bilayer used to derive Eqs. (1)–(3). It shows a Ni and Al thin film with NiAl periodically penetrating the Al film where grain boundaries would be present.  $\lambda_{Al}$  is the average width of an Al grain while  $\lambda_{NiAl}$  is the average width of high Ni activity in the Al grain boundary, both derived from the data shown in Fig. 7b. The Al and Ni layer thicknesses,  $D_{Al}$  and  $D_{Ni}$ , were taken from the STEM images shown in Fig. 7a.

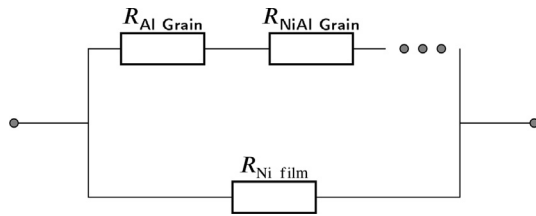


**Fig. 12.** A circuit diagram representation of the schematic of a Ni/Al bilayer shown in Fig. 11 from which Eqs. (1)–(3) were derived. The Ni and Al layers are placed in parallel. While the Ni layer is treated as a homogeneous body, the Al and NiAl grains within the Al layer are placed in series and repeated through the length of the coil by an amount equal to the total coil length divided by the average length of a pair of Al and NiAl grains.

as shown in Fig. 12. The total resistance,  $R_T$ , of the third outermost coil lane that was measured can be calculated as follows,

$$R_T = \frac{1}{n/R_{Al\ film} + n/R_{Ni\ film}} \quad (1)$$

where  $n$  is the number of bilayers (in our case 3), and  $R_{Al\ film}$  and  $R_{Ni\ film}$  are the total resistances of a single Al and Ni film, respectively.  $R_{Ni\ film}$  can be calculated directly from the resistivity of Ni,  $\rho_{Ni}$ , as follows,

$$R_{Ni\ film} = \frac{\rho_{Ni}\lambda_T}{wD_{Ni}} \quad (2)$$

where  $\lambda_T$  is the total length of the coil (measured to be about 3.7 mm), and  $w$  is the width of the coil which was 90  $\mu\text{m}$ . For  $R_{Al\ film}$ , the resistances of Al and NiAl grains were added up taking into account their average lengths derived from the data shown in Fig. 7b as follows,

$$R_{Al\ film} = \left( \frac{\rho_{Al}\lambda_{Al} + \rho_{NiAl}\lambda_{NiAl}}{wD_{Al}} \right) \frac{\lambda_T}{\lambda_{Al} + \lambda_{NiAl}} \quad (3)$$

The resistivity of NiAl has been found to be quite sensitive to the concentration of either metal, showing a low point of about  $1 \times 10^{-7}\Omega\text{m}$  which rises quickly to  $2 \times 10^{-7}\Omega\text{m}$  when Al concentration is decreased to 48% or increased to 51% [17]. Due to this high level of sensitivity, a compromise value of  $1.5 \times 10^{-7}\Omega\text{m}$  for  $\rho_{NiAl}$  was taken. The results show that when  $\lambda_{NiAl}$  was increased from 0 to 52 nm, total resistance increased by 1.27  $\Omega$ . This matches up very well with the data shown in Fig. 10, where if a straight line is propagated from the resistance line before the onset of peak 1 and compared with the resistance value measured after peak subsidence at about 311  $^\circ\text{C}$ , we see a difference of about 1.4  $\Omega$ . The most significant simplifying assumption taken in this calculation is that the Al grains and their Ni rich grain boundaries extend along the width of the coil lane (90  $\mu\text{m}$ ). Though this is of course not the case, even when these Al grains are staggered the Ni rich layer enveloping them would still prevent any low resistance paths from remaining in the Al film.

## 5. Conclusion

While there exists work in the literature that analyze the relationship of resistance changes to evolutions in sample microstructure induced by thermal pulses [18–20], most work on materials subjected to fast thermal pulses study phase changes using calorimetric methods. This is a fairly accessible and far more sensitive technique than resistance measurements alone as evidenced by the popularity of nanocalorimetry and recent advances pushing into picowatt resolutions [21]. However, as mentioned in the work of Zhang et al. [18], there are many microstructural evolutions such as grain growth, precipitation, and grain boundary diffusion that

involve only a miniscule amount of phase change that are interesting to the study of heterogeneous microstructures.

The method described here presents a simple but powerful technique, shown in this work to be sensitive to specific and interesting structural changes in multilayer Ni/Al thin films, that is capable of high heating rates (up to  $10^4$  K/s were achieved), a high throughput architecture, and the possibility for applications to nonconducting materials such as ceramics using indirect heating [22]. With the primary assumption that pulsing the calibration and sample with the same power results in the same temperature contributing only a minor error in temperature measurement, the direct thermocouple measurements during the calibration procedure provide a higher accuracy than pyrometry and a larger temperature range than melting point analysis. Accurate temperature measurements remain a common challenge in calorimetry. The authors believe that the heating rates and structural sensitivity of this technique would be a potent addition to the phase sensitivity of calorimetric methods in studying materials subjected to fast thermal pulses.

## 6. Data Availability

The raw and processed data required to reproduce these findings are available to download from this link.

## Declaration of Competing Interest

The authors declare that they have no known competing financial interests or personal relationships that could have appeared to influence the work reported in this paper.

## Acknowledgements

K.W. and M.S. gratefully acknowledge the financial support of the German Research Foundation (DFG) within the Emmy-Noether-Program (funding number: WO 2198/1–1).

## References

- [1] H. Zhang, D. Lee, Y. Shen, Y. Miao, J. Bae, Y. Liu, J. Schroers, Y. Xiang, J.J. Vlassak, Combinatorial temperature resistance sensors for the analysis of phase transformations demonstrated for metallic glasses, *Acta Mater.* 156 (2018) 486–495.
- [2] F. Yi, D.A. Lavan, Nanocalorimetry: Exploring materials faster and smaller (sep 2019). doi:10.1063/1.5098297.
- [3] L. Alawieh, T.P. Weihs, O.M. Knio, A generalized reduced model of uniform and self-propagating reactions in reactive nanolaminates, *Combust. Flame* 160 (9) (2013) 1857–1869, <https://doi.org/10.1016/j.combustflame.2013.03.016>.
- [4] T. Neuhauser, G. Tinti, H. Leiste, N. Casati, S. Ulrich, M. Stüber, K. Woll, The role of two-stage phase formation for the solid-state runaway reaction in Al/Ni reactive multilayers, *Appl. Phys. Lett.* 117 (1) (2020), <https://doi.org/10.1063/5.0011338>.
- [5] G.M. Fritz, J.A. Grzyb, O.M. Knio, M.D. Grapes, T.P. Weihs, Characterizing solid-state ignition of runaway chemical reactions in Ni-Al nanoscale multilayers under uniform heating, *J. Appl. Phys.* 118 (13) (2015) 135101, <https://doi.org/10.1063/1.4931666>.
- [6] G.M. Fritz, S.J. Spey, M.D. Grapes, T.P. Weihs, Thresholds for igniting exothermic reactions in Al/Ni multilayers using pulses of electrical, mechanical, and thermal energy, *J. Appl. Phys.* 113 (1) (2013) 014901, <https://doi.org/10.1063/1.4770478>.
- [7] E.G. Colgan, C. Cabral, D.E. Kotecki, Activation energy for CoSi and CoSi<sub>2</sub> formation measured during rapid thermal annealing, *J. Appl. Phys.* 77 (2) (1998) 614, <https://doi.org/10.1063/1.359046>.
- [8] L.H. Allen, G. Ramanath, S.L. Lai, Z. Ma, S. Lee, D.D. Allman, K.P. Fuchs, 1 000 000C/s thin film electrical heater: In situ resistivity measurements of Al and Ti/Si thin films during ultra rapid thermal annealing, *Appl. Phys. Lett.* 64 (4) (1994) 417–419, <https://doi.org/10.1063/1.111116>.
- [9] P. Swaminathan, B.G. Burke, A.E. Holness, B. Wilthan, L. Hanssen, T.P. Weihs, D. A. Lavan, Optical calibration for nanocalorimeter measurements, *Thermochim. Acta* 522 (1–2) (2011) 60–65, <https://doi.org/10.1016/j.TCA.2011.03.006>.
- [10] M.D. Grapes, T. Lagrange, K. Woll, B.W. Reed, G.H. Campbell, D.A. Lavan, T.P. Weihs, In situ transmission electron microscopy investigation of the interfacial reaction between Ni and Al during rapid heating in a nanocalorimeter, *APL Materials* 2 (11) (2014) 116102, <https://doi.org/10.1063/1.4900818>.

- [11] T. Neuhauser, G. Tinti, H. Leiste, N. Casati, M. Stüber, K. Woll, Analysis of the reaction runaway in Al/Ni multilayers with combined nanocalorimetry and time-resolved X-ray diffraction, *Acta Mater.* 195 (2020) 579–587, <https://doi.org/10.1016/j.actamat.2020.05.035>.
- [12] F. Yi, J.B. Delisio, M.R. Zachariah, D.A. Lavan, Nanocalorimetry-Coupled Time-of-Flight Mass Spectrometry: Identifying Evolved Species during High-Rate Thermal Measurements, *Anal. Chem.* 87 (2015) 35, <https://doi.org/10.1021/acs.analchem.5b01872>.
- [13] M.D. Grapes, T. Lagrange, L.H. Friedman, B.W. Reed, G.H. Campbell, T.P. Weihs, D.A. Lavan, Combining nanocalorimetry and dynamic transmission electron microscopy for in situ characterization of materials processes under rapid heating and cooling, *Review of Scientific Instruments* 85 (8) (aug 2014). doi:10.1063/1.4892537.
- [14] H.E. Kissinger, Variation of peak temperature with heating rate in differential thermal analysis, *J. Res. Natl. Bureau of Stand.* 57 (4) (1956) 217, <https://doi.org/10.6028/jres.057.026>.
- [15] D. Smeets, J. Demeulemeester, D. Deduytsche, C. Detavernier, C.M. Comrie, C.C. Theron, C. Lavoie, A. Vantomme, Simultaneous real-time x-ray diffraction spectroscopy, Rutherford backscattering spectrometry, and sheet resistance measurements to study thin film growth kinetics by Kissinger plots, *J. Appl. Phys.* 104 (10) (2008) 103538, <https://doi.org/10.1063/1.3021110>.
- [16] H. Miura, E. Ma, C.V. Thompson, Initial sequence and kinetics of silicide formation in cobalt/amorphous-silicon multilayer thin films, *J. Appl. Phys.* 70 (8) (1998) 4287, <https://doi.org/10.1063/1.349106>.
- [17] Y. Yamaguchi, D.A. Kiewit, T. Aoki, Electrical Resistivity of NiAl, CoAl, NiGa, and CoGa, *J. Appl. Phys.* 39 (1968) 231, <https://doi.org/10.1063/1.1655738>.
- [18] S.L. Zhang, J.M. Harper, C. Cabral, F.M. D'Heurle, In situ resistivity study of copper–cobalt films: precipitation, dissolution and phase transformation, *Thin Solid Films* 401 (1–2) (2001) 298–305, [https://doi.org/10.1016/S0040-6090\(01\)01610-8](https://doi.org/10.1016/S0040-6090(01)01610-8).
- [19] S.L. Zhang, F.M. D'Heurle, Kinetic studies of intermetallic compound formation by resistance measurements, *Thin Solid Films* 256 (1–2) (1995) 155–164, [https://doi.org/10.1016/0040-6090\(94\)06288-9](https://doi.org/10.1016/0040-6090(94)06288-9).
- [20] E.G. Colgan, F.M. D'Heurle, Kinetics of silicide formation measured by in situ ramped resistance measurements, *J. Appl. Phys.* 79 (8) (1998) 4087, <https://doi.org/10.1063/1.361771>.
- [21] J. Bae, J. Zheng, H. Zhang, P.J. Foster, D.J. Needleman, J.J. Vlassak, A micromachined picocalorimeter sensor for liquid samples with application to chemical reactions and biochemistry, *Adv. Sci.* 8 (5) (2021) 2003415, <https://doi.org/10.1002/ADVS.202003415>.
- [22] J. Zheng, H. Zhang, Y. Miao, S. Chen, J.J. Vlassak, Temperature-resistance sensor arrays for combinatorial study of phase transitions in shape memory alloys and metallic glasses, *Scripta Mater.* 168 (2019) 144–148.